Generalized homogenization model of piezoelectric materials for ultrasonic transducer applications

Fidéle Léopold Hanse Wampo, Richard Ntenga, Joseph Yves Effa, Yuri Lapusta, Guy Edgar Ntamack, Pierre Maréchal

Generalized homogenization model of piezoelectric materials for ultrasonic transducer applications

F.L. Hanse Wampo[1, 2], R. Ntenga[3], J.Y. Effa[2], Y. Lapusta[4], G.E. Ntamack[1, 2], P. Maréchal[5]

[1]Groupe de Mécanique des Matériaux et l'Acoustique (GMMA), Université de Ngaoundéré, BP : 454-Cameroun.

[2]Faculté des Sciences-Département de Physique, Université de Ngaoundéré-Cameroun.

[3]Laboratoire d'Analyses Simulations et Essais, Institut Universitaire de Technologie, Université de Ngaoundéré-Cameroun.

[4]Institut Pascal-UMR 6602-UCA/CNRS/SIGMA, Université de Clermont Auvergne- France.

[5]Laboratoire Ondes et Milieux Complexes (LOMC), UMR 6294 CNRS, Université du Havre, France.

Corresponding author: fidelehans@yahoo.fr

Abstract: Although piezocomposite (PC) materials have increasingly attracted researchers, there is still a need to properly and easily derive their properties. We develop a generalized homogenization model (GHM) that accounts for Smith and Cha approaches to evaluate the equivalent characteristics of piezocomposites. This method could be applied to all connectivities patterns, but restricted herein to 2-2 and 1-3 piezocomposites for comparison with Smith (1-3) and Cha (2-2) analytical results. In the proposed GHM is a parameter θ, is changed for various connectivities. The 1-3 and 2-2 PZT-7A/Araldite D (PCs) data are used and equivalent characteristics of these Pcs are determined as function of volume fraction of PZT-7A piezoelectric. Results show that the electromechanical coefficients are well fitted by Voigt and Reuss models. Results obtained for some parameters show that the proposed GHM is consistent with the analytical existing models used for the 1-3 and 2-2 connectivities and is in line with measured values from Chan and Unsworth (1989). Based on the GHM 2-2 configuration results of piezocomposite materials, the electroacoustic responses of transducers having some of these properties are simulated using the KLM model. A performance trade-off was chosen, resulting in an improved thickness coupling coefficient and a lowered acoustical impedance, and a similar approach as that on a pure PZT-7A.

Keywords: Piezoelectric materials, generalized homogenization models, material connectivity, ultrasonic transducers.

1. Introduction

The use of ultrasonic waves for inspection, control and material characterization is nowadays widely explored. Piezoelectric materials are the most used as active material for ultrasound applications and both their compositions and fabrication methods have known strong developments, especially in submarine detection systems and biomedical imaging [1–4]. In addition, the use of these materials is likely to expand to mobile and embedded electronics. Applications of piezoelectric materials require improvement of their characteristics. The electromechanical behavior study of composite materials necessarily involves multi scale methods [5–7] that are generally difficult to implement. Therefore, numerical modeling is preferred when studying their micro-macro mechanical behavior.

Various works dealing with homogenization of PC properties are found in the literature. Especially, in linear elasticity, the upper and lower bounds of homogenization models are the sum of the stiffness coefficients (Voigt) [8] and the reciprocal compliance coefficients of the constituent phases (Reuss) [9]. Following this trend, Hashimoto and Yamaguchi [10] proposed an analytical method termed the matrix method for calculating equivalent composite elastic coefficients. Their method was further applied to the case of the 2-2 and 1-3 PC patterns, assuming that the stress and electric displacement are continuous in the perpendicular direction to the interface and that the strain and electric fields are continuous in the parallel direction to the interface. Levassort et al. [11] also focused on the matrix method; they described a generic formalism that can be easily transposed to other connectivities, the 0-3 PC pattern for instance was used for illustration purposes. The matrix method also used to evaluate all of the effective parameters of pure 0-3 and 3-3 piezocomposites, then it is used to obtain the effective properties of a 3-3(0-3) composite [12]. The model developed by Smith [13] is valid for a PC with a lateral spatial scale sufficiently fine for the material to be treated as a homogeneous continuum. To determine the elastic, piezoelectric and dielectric coefficients, Smith [13] proposed 3D relationships for the polymer matrix phase

and the piezoelectric ceramic phase . The assumption of an isostrain in x_1 and x_2 directions for the matrix and the piezoelectric phases was used ($S_1^{p,c} = S_2^{p,c}$) (see Fig. 1 and 2 for the definition of axis). Cha [14] assumed that the 2 direction length of the 2-2 PC is infinite compared with that of the x_1 direction. Likewise, the isostrain hypothesis about the x_2 direction in the matrix and the piezoelectric phases are used. The said strain can be assumed null ($S_2^p = S_2^c = 0$). Levin et al. [15] analyzed the effective properties of electroelastic composites using the self-consistent and asymptotic homogenization methods. Their results are valid for high contrasts among all the physical parameters (ceramic fiber and polymer matrix), and to mention that the explicit self-consistent equations provided with the effective field hypothesis yields the same equations as the Mori-Tanaka method. Della et al. [6] studied the performance of 1-3 PC pattern that consist of an active and passive phases using the Mori-Tanaka model (MTM) [16]. They reported that, electromechanical parameters obtained when an active polymer phase is used, can improve the performance of the studied hydrophone. For the 1-3 and 2-2 PCs, the electroacoustic responses of transducers having some of those properties are simulated using the KLM model [3], consisting in an electrical equivalent model which takes into account both the acoustic properties of the front and rear surrounding media, as well as the electrical environment. As a result, an optimal design of transducer aimed at ultrasound imaging applications is proposed as a dedicated imaging performance index, elaborated through a trade-off between sensitivity and bandwidth [17,18]. Topolov et al. [19,20] also applied the MTM, to derive the 0-3 PC type made up of a relaxor-ferroelectric single crystals, after they are evaluated the problems of piezocomposite sensitivity based on ferroelectric ceramics and figures of merit [21].

Wenkang Qi and Wenwu Cao [22], carried out the finite elements analysis (FEA) and experiments on resonance in thickness mode of the 2-2 PC sensors. It should be noted that the effective average theory (EAT) yields good results when the a / l aspect ratio (where "a'' donates the dimension along the direction x_3, and "l" is the piezoelectric rod dimension perpendicular to the direction x_3) is lower than 0.4; but for aspect ratios higher than 0.4, the predicted EAT resonance values will be larger than the natural frequencies of the transducers. Madhusudhana [23] carried out numerical and analytical studies on the 1-3 PZT 7A/Araldite D PC. It was found that the effective properties are sensitive to a / l only for high volume fraction. It was also reported that the relative permittivity is almost independent on a / l no matter the volume fraction. Mai Pham Thi et al. [1] conducted a surface study of a single crystal PMN-PT 0-3 and 1-3 PC used as a transducer. They reported that the predicted coupling coefficient in thickness mode is twofold that of the standard PZT material. Yanjun Zhang et al., [24] had proposed a theoretical model which can reproduce the effective parameters of 1-3 piezoelectric composites with a sandwich polymer in the thickness mode, and theirs assumptions are made on the basis of uniform field theories and the rule of mixtures. The measured electromechanical coupling factor was improved by more than 9.8% over the PZT/resin 1-3 piezoelectric composite. Sakthivel et al. [25] carried out a parametric study, to investigate the effects of variations in the poling characteristics of the fiber and matrix phase on the overall thermo-electro-mechanical behavior of a 1-3 piezocomposite. In their study, an analytical method accounting for the "parallel" and "series" theory was introduced for the 1-3 PC. They showed that the variations of the elastic, piezoelectric and dielectric constant with the volume fraction of the ceramic rod are nonlinear.

Electromechanical coupling coefficient directly reflects the electromechanical energy conversion capability of a piezoelectric device. It is an important parameter for the performance of piezoelectric transducers, thus Wang et al. [7] established a unified formula to test the effect of the "kerf filler" (which is the polymer matrix phase of the piezocomposite in this case) on the electromechanical coupling coefficient of the 1-3 PCs. With regard to the influence of the "kerf filler" on the electromechanical coupling coefficient, only the 2-2 PC was studied. As a general rule, they concluded that the coupling coefficient increases with the decrease in the elastic coefficient of the "kerf filler". Wang extended the modified series and parallel model to 1-3-2 PC type and calculated the effective parameters of the 1-3-2 composites [26], [27]. Zhou et al. [4], worked on a single piezoelectric crystal of the 1-3 PCs without lead material for ultrasonic sensor. A comparison of these results and their corresponding finite element estimates was further done by Martinez et al. [28]. Geers et al. [29] worked on multi-scale computational homogenization. The effective electromechanical coefficients have been calculated by Berger et al., [30] using the asymptotic homogenization method (AHM) for six different fiber volume fractions. Avellaneda et al. [31] proposed an approach using an effective medium to evaluate the performance of 1-3 polymer/piezoelectric ceramic composites for hydrophone applications. He shows that the composite was treated as an equivalent homogeneous continuum or effective medium, and its effective properties were computed from the effective response tensor. Dunn and Taya [26, 27] made an analysis of piezoelectric composite materials containing ellipsoidal inhomogeneities. Some authors focused on various other problems such as the elastic

properties of reinforced solids: the determination of the elastic field of an ellipsoidal inclusion and related problems [34], some theoretical principles [35], the average stress in matrix and average elastic materials energy with imperfect inclusions [36]. Pakam et al. [37] developed an analytical model based on a theoretical model of 1-3-2 piezocomposites and studied the effect of the ceramic base volume fraction on the overall 1-3-2 magneto-electro-elastic composite behavior; in their study, the simulated results compared with the results from finite element methods.

For each PC pattern there exists a specific model to compute the PCs effective coefficients. In our study, we are interested in having a GHM that can be applied to all connectivity patterns by replacing a parameter, say θ, specific to each PC pattern. Numerical simulations based on the new model are to be implemented for validation purposes.

2. Connectivity

To define how phases are coupled, Newnham et al. [38] introduced the concept of connectivity. The piezocomposites are classified according to their connectivity (such as 2-2, 1-3, 0-3, 3-3 etc…), the first phase is by convention the piezoelectric phase. Connectivity is defined as the number of dimensions through which the material is continuous. For the 2-2 piezocomposites, two representations (fig.1a, fig.1b) are possible and in this paper, we have homogenized the 2-2 parallel model (fig.1b) whose piezoelectric phase is poled in its longitudinal direction (direction x_3).

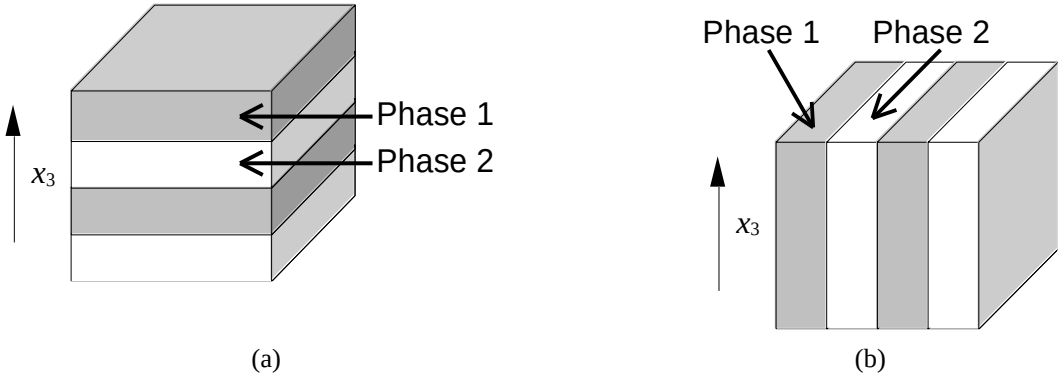

Figure 1 – Basic piezocomposite cell for the 2-2 (a) series and (b) parallel connectivities.

The 1-3 piezocomposites consist of the active piezoelectric rods (continuous connectivity in one dimension) which are embedded into the passive matrix that has continuous connectivity along all three dimensions. This configuration is illustrated in fig. 2 and the piezoelectric phase is poled along its a longitudinal direction (direction x_3).

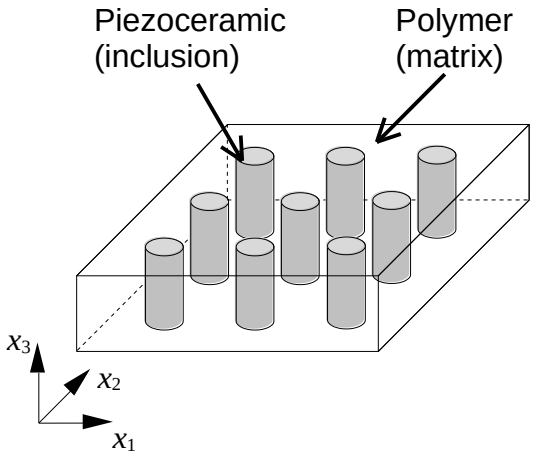

Figure 2 – Schematic representation of 1-3 piezocomposite made from PZT rods in a polymer matrix.

3. Development of generalized homogenization model

3.1. Constitutive equations

For an infinitesimal strain, the components of the second order strain tensor are defined by the following equation:

$$S_{ij} = \frac{1}{2}\left(u_{i,j} + u_{j,i}\right) \qquad \text{with} \qquad u_{i,j} = \frac{\partial u_i}{\partial x_j} \tag{1}$$

where S_{ij} are the strain tensor components, the indices i and j are equal to 1, 2 or 3, u_i is a component of the displacement vector $u(x)$ along the x_i axis.

In a piezoelectric material, electrical and mechanical phenomena interact, resulting in electromechanical effects. Neglecting the pyroelectric effect, the constitutive equation of piezoelectricity can be written as a generalized Hooke's law:

$$\binom{T}{D} = \begin{bmatrix} c^E & -e^t \\ e & \epsilon^S \end{bmatrix} \binom{S}{E} \tag{2}$$

where the contracted symmetric matrix notation is used. Two suffixes are abbreviated in to single one according to the following scheme:

Tensor notation	11	22	33	23 (or 32)	13 (or 31)	12 (or 21)
Matrix notation	1	2	3	4	5	6

T is the stress vector which includes all the components of the stress tensor $T = (T_1, T_2, T_3, T_4, T_5, T_6)$ (see Eqs. 3-11). In the same way, the strain vector is $S = (S_1, S_2, S_3, S_4, S_5, S_6)$, the electrical field vector is $E = (E_1, E_2, E_3)$ and the electrical displacement field vector is $D = (D_1, D_2, D_3)$. c^E the stiffness components at constant electrical field, e the piezoelectric components (where e^t is the transpose of the piezoelectric components), and ϵ^S the dielectric components at constant strain, and the parameters of the homogenized material are noted with an over-stricke. In the MKS system, the variables of the different properties have the following units [32]:

$[T]$ is in $\mathrm{N/m^2}$, $[S]$ is in $\mathrm{m/m}$, $[D]$ is in $\mathrm{N/(Vm)}$, $[E]$ is in $\mathrm{V/m}$,
$[c^E]$ is in $\mathrm{N/m^2}$, $[e]$ is in $\mathrm{N/(Vm) = C/m^2}$, $[\epsilon^S]$ is in $\mathrm{N/V^2 = C^2/(Nm^2)}$.

3.2. Model formulation

A generalized homogenization model (GHM) developed here is based on the Smith and Cha models. Whereas the uniform field theories developed by Y. Benveniste and G. J. Dvorak [39] are made on the basis of the rule of mixtures of Voigt and Reuss. The constitutive relations for the components phases give the stress and electric displacement at every point (x_1, x_2, x_3) within the plate. To apply boundary conditions and the conditions of continuity between the two phases, the constitutive equations of Smith and Cha models are considered when one use the two concerned connectivities. The polymer phase is an isotropic homogeneous medium that is piezoelectrically inactive, thus for (x_1, x_2, x_3) within the polymer phase we have:

$$\begin{bmatrix} T_1^p \\ T_2^p \\ T_3^p \\ T_4^p \\ T_5^p \\ T_6^p \\ D_1^p \\ D_2^p \\ D_3^p \end{bmatrix} = \begin{bmatrix} c_{11} & c_{12} & c_{13} & 0 & 0 & 0 & 0 & 0 & 0 \\ c_{12} & c_{11} & c_{13} & 0 & 0 & 0 & 0 & 0 & 0 \\ c_{13} & c_{13} & c_{33} & 0 & 0 & 0 & 0 & 0 & 0 \\ 0 & 0 & 0 & c_{44} & 0 & 0 & 0 & 0 & 0 \\ 0 & 0 & 0 & 0 & c_{44} & 0 & 0 & 0 & 0 \\ 0 & 0 & 0 & 0 & 0 & c_{66} & 0 & 0 & 0 \\ 0 & 0 & 0 & 0 & 0 & 0 & \epsilon_{11} & 0 & 0 \\ 0 & 0 & 0 & 0 & 0 & 0 & 0 & \epsilon_{11} & 0 \\ 0 & 0 & 0 & 0 & 0 & 0 & 0 & 0 & \epsilon_{33} \end{bmatrix} \begin{bmatrix} S_1^p \\ S_2^p \\ S_3^p \\ S_4^p \\ S_5^p \\ S_6^p \\ E_1^p \\ E_2^p \\ E_3^p \end{bmatrix} \tag{3a-i}$$

We consider the piezoelectric ceramics to be poled along the rods perpendicular to the plate, hence for (x_1, x_2, x_3) in the ceramic phase we have:

$$\begin{bmatrix} T_1^c \\ T_2^c \\ T_3^c \\ T_4^c \\ T_5^c \\ T_6^c \\ D_1^c \\ D_2^c \\ D_3^c \end{bmatrix} = \begin{bmatrix} c_{11}^E & c_{12}^E & c_{13}^E & 0 & 0 & 0 & 0 & 0 & -e_{31} \\ c_{12}^E & c_{11}^E & c_{13}^E & 0 & 0 & 0 & 0 & 0 & -e_{31} \\ c_{13}^E & c_{13}^E & c_{33}^E & 0 & 0 & 0 & 0 & 0 & -e_{31} \\ 0 & 0 & 0 & c_{44}^E & 0 & 0 & 0 & -e_{15} & 0 \\ 0 & 0 & 0 & 0 & c_{44}^E & 0 & -e_{15} & 0 & 0 \\ 0 & 0 & 0 & 0 & 0 & c_{66}^E & 0 & 0 & 0 \\ 0 & 0 & 0 & 0 & e_{15} & 0 & \epsilon_{11}^S & 0 & 0 \\ 0 & 0 & 0 & e_{15} & 0 & 0 & 0 & \epsilon_{11}^S & 0 \\ e_{31} & e_{31} & e_{33} & 0 & 0 & 0 & 0 & 0 & \epsilon_{33}^S \end{bmatrix} \begin{bmatrix} S_1^c \\ S_2^c \\ S_3^c \\ S_4^c \\ S_5^c \\ S_6^c \\ E_1^c \\ E_2^c \\ E_3^c \end{bmatrix} \quad \text{(4a-i)}$$

Solving Eqs (4a-4i) for material properties necessitates several approximations used for the derivation of the thickness-mode oscillations in 1-3 PC [13]. In particular, it is assumed that the strain and electric fields are independent of the individual ceramic and polymer phases, and the electric field is applied only to the x_3 direction in thickness mode oscillations. These approximations are as follows [13,14]:

* Based on the subsequent approximation in which the ceramic and the polymer move together in a uniform thickness oscillation, the vertical strains are the same in both phases, i.e.,

$$S_3^p = S_3^c = \bar{S}_3 \quad (5)$$

* In addition, since the faces of the composite plates are electroded and thus equipotentials, the electric field is assumed to be the same in both phases, i.e.,

$$E_3^p = E_3^c = \bar{E}_3 \quad (6)$$

* It is also assumed that the lateral stress (the stress on the lateral faces) is the same in both phases. Also, the ceramic's lateral strain is compensated by a complementary strain of the polymer, so that the composite as a whole is laterally clamped. Therefore,

$$T_i^p = T_i^c = \bar{T}_i, \; i = 1, \text{or} \;\; 2 \quad (7)$$

$$\bar{S}_i = \nu S_i^c + \bar{\nu} S_i^p = 0, \; i = 1, \text{or} \;\; 2 \quad (8)$$

where ν is the ceramic volume fraction, and $\bar{\nu} = 1 - \nu$ is the volume fraction of polymer. It can also be assumed that the total stress and electric displacement are obtained by averaging the above contributions of the constituent phases. Since the lateral periodicity is sufficiently fine, we find the effective total stress and electric displacement by averaging over the contributions of the constituent phases. Hence we have:

$$\bar{T}_3 = \nu T_3^c + \bar{\nu} T_3^p, \quad (9)$$

$$\bar{D}_3 = \nu D_3^c + \bar{\nu} D_3^p. \quad (10)$$

From Eq (7), $T_1^p = T_1^c$ we can deduce:

$$c_{11} S_1^p + c_{12} S_2^p + c_{12} S_3^p = c_{11}^E S_1^c + c_{12}^E S_2^c + c_{13}^E S_3^c - e_{31} E_3^c \quad (11)$$

From Eq (8), we have:

$$S_i^p = -\frac{\nu}{\bar{\nu}} S_i^c \quad (12)$$

Using Eq (12) in (11) we have:

$$\frac{\nu}{\bar{\nu}}(c_{11} + c_{11}^E) S_1^c + \left(\frac{\nu}{\bar{\nu}} c_{12} + c_{12}^E\right) S_2^c = (c_{12} - c_{13}^E)\bar{S}_3 + e_{31}\bar{E}_3 \quad (13)$$

In the same way,

$$c_{12} S_1^p + c_{11} S_2^p + c_{12} \bar{S}_3 = c_{12}^E S_1^c + c_{11}^E S_2^c + c_{13}^E \bar{S}_3 - e_{31}\bar{E}_3 \quad (14)$$

$$\left(\frac{\nu}{\bar{\nu}} c_{12} + c_{12}^E\right) S_1^c + \left(\frac{\nu}{\bar{\nu}} c_{11} + c_{11}^E\right) S_2^c = (c_{12} - c_{13}^E)\bar{S}_3 + e_{31}\bar{E}_3 \quad (15)$$

After some calculation, by combining Eqs (13) and (15), we obtain:

$$\begin{bmatrix} S_1^c \\ S_2^c \end{bmatrix} = \begin{bmatrix} \alpha(c_{12} - c_{13}^E) & -\beta(c_{12} - c_{13}^E) \\ -\beta(c_{12} - c_{13}^E) & \alpha(c_{12} - c_{13}^E) \end{bmatrix} \begin{bmatrix} \bar{S}_3 \\ \bar{S}_3 \end{bmatrix} + \begin{bmatrix} \alpha(e_{31}) & -\beta(e_{31}) \\ -\beta(e_{31}) & \alpha(e_{31}) \end{bmatrix} \begin{bmatrix} \bar{E}_3 \\ \bar{E}_3 \end{bmatrix} \quad (16)$$

As a result, the displacement components $S_1^c = S_2^c$ are identified as equal along the axis 1 and axis 2.

Combining Eqs (16) and (4c) gives:

$$T_3^c = c_{13}^E[(\alpha - \beta)(c_{12} - c_{13}^E)\bar{S}_3 + (\alpha - \beta)e_{31}\bar{E}_3] + c_{13}^E[(\alpha - \beta)(c_{12} - c_{13}^E)\bar{S}_3 + (\alpha - \beta)e_{31}\bar{E}_3] + c_{33}^E \bar{S}_3 - e_{33}\bar{E}_3 \quad (17)$$

$$T_3^c = [2c_{13}^E(\alpha - \beta)(c_{12} - c_{13}^E) + c_{33}^E]\bar{S}_3 + [2c_{13}^E(\alpha - \beta)e_{31} - e_{33}]\bar{E}_3 \quad (18)$$

$$T_3^p = c_{12} S_1^p + c_{12} S_2^p + c_{11} S_3^p \quad (19)$$

Combining Eqs (12) and (19) gives:

$$T_3^p = -\frac{\nu}{\bar{\nu}} c_{12} S_1^c - \frac{\nu}{\bar{\nu}} c_{12} S_2^c + c_{11} \bar{S}_3 \tag{20}$$

Combining Eqs (16) and (20) gives:

$$T_3^p = [-2\frac{\nu}{\bar{\nu}} c_{12}(\alpha - \beta)(c_{12} - c_{13}^E) + c_{11}]\bar{S}_3 - 2\frac{\nu}{\bar{\nu}} c_{12}(\alpha - \beta) e_{31} \bar{E}_3 \tag{21}$$

Combining Eqs (18) and (21) gives the final system:

$$\begin{cases} T_3^c = [2c_{13}^E(\alpha - \beta)(c_{12} - c_{13}^E) + c_{33}^E]\bar{S}_3 + [2c_{13}^E(\alpha - \beta)e_{31} - e_{33}^E]\bar{E}_3 \\ T_3^p = \left[-2\frac{\nu}{\bar{\nu}} c_{12}(\alpha - \beta)(c_{12} - c_{13}^E) + c_{11}\right]\bar{S}_3 - 2\frac{\nu}{\bar{\nu}} c_{12}(\alpha - \beta) e_{31} \bar{E}_3 \end{cases} \tag{22}$$

Combining Eqs (22) and (9) gives:

$$\begin{aligned} \bar{T}_3 = \nu([2c_{13}^E(\alpha - \beta)(c_{12} - c_{13}^E) + c_{33}^E]\bar{S}_3 + [2c_{13}^E(\alpha - \beta)e_{31} - e_{33}]\bar{E}_3) \\ +\bar{\nu}(\left[-2\frac{\nu}{\bar{\nu}} c_{12}(\alpha - \beta)(c_{12} - c_{13}^E) + c_{11}\right]\bar{S}_3 - 2\frac{\nu}{\bar{\nu}} c_{12}(\alpha - \beta) e_{31} \bar{E}_3) \end{aligned} \tag{23}$$

$$\begin{aligned} \bar{T}_3 = [-2\nu(\alpha - \beta)(c_{13}^E - c_{12})^2 + \nu c_{33}^E + \bar{\nu} c_{11}]\bar{S}_3 \\ +[2\nu(\alpha - \beta)(c_{13}^E - c_{12})e_{31} - \nu e_{33}]\bar{E}_3 \end{aligned} \tag{24}$$

Combining Eqs (3i) and (4i) gives the system:

$$\begin{cases} D_3^p = \epsilon_{11} E_3^p = \epsilon_{11} \bar{E}_3 \\ D_3^c = e_{31} S_1^c + e_{31} S_2^c + e_{33} S_3^c + \epsilon_{33}^S E_3^c \end{cases} \tag{25}$$

Combining Eqs (16) and (4i):

$$D_3^c = [2e_{31}(\alpha - \beta)(c_{12} - c_{13}^E) + e_{33}]\bar{S}_3 + [2(\alpha - \beta)e_{31}^2 + \epsilon_{33}^S]\bar{E}_3 \tag{26}$$

Replacing D_3^C of Eq (26), by its final expression, Eq (25) rewrites:

$$\begin{cases} D_3^p = \epsilon_{11} \bar{E}_3 \\ D_3^c = [2e_{31}(\alpha - \beta)(c_{12} - c_{13}^E) + e_{33}]\bar{S}_3 + [2(\alpha - \beta)e_{31}^2 + \epsilon_{33}^S]\bar{E}_3 \end{cases} \tag{27}$$

Combining Eqs (27) and (10) gives:

$$\bar{D}_3 = [2\nu e_{31}(\alpha - \beta)(c_{12} - c_{13}^E) + \nu e_{33}\bar{S}_3 + [2\nu(\alpha - \beta)e_{31}^2 + \nu\epsilon_{33}^S + \bar{\nu}\epsilon_{11}]\bar{E}_3 \tag{28}$$

Thus the constitutive piezoelectricity relationship gives:

$$\bar{T}_3 = \bar{c}_{33}^E \bar{S}_3 - \bar{e}_{33} \bar{E}_3 \tag{29}$$

$$\bar{D}_3 = \bar{e}_{33} \bar{S}_3 + \bar{\epsilon}_{33}^S \bar{E}_3 \tag{30}$$

By identification, we have:

$$\bar{c}_{33}^E = \nu[c_{33}^E - 2(\alpha - \beta)(c_{13}^E - c_{12})^2] + \bar{\nu} c_{11} \tag{31}$$

$$\bar{e}_{33} = \nu[e_{33} - 2e_{31}(\alpha - \beta)(c_{13}^E - c_{12})] \tag{32}$$

$$\bar{\epsilon}_{33}^S = \nu[\epsilon_{33}^S - 2(\alpha - \beta)e_{31}^2] + \bar{\nu} c_{11} \tag{33}$$

Let's denote $\theta = \alpha - \beta$, and Eqs (31), (32) and (33) become:

$$\bar{c}_{33}^E = \nu[c_{33}^E - 2\theta(c_{13}^E - c_{12})^2] + \bar{\nu} c_{11} \tag{34}$$

$$\bar{e}_{33} = \nu[e_{33} - 2e_{31}\theta(c_{13}^E - c_{12})] \tag{35}$$

$$\bar{\epsilon}_{33}^S = \nu[\epsilon_{33}^S - 2\theta e_{31}^2] + \bar{\nu} c_{11} \tag{36}$$

Eventually, the generalized homogenization approach described above is applicable for the moment to the 1-3 and 2-2 PC connectivities. The proposed model enables to study the influence of the volume fraction of the two connectivities 1-3 and 2-2. The θ ($\theta = \alpha - \beta$), parameter even makes it possible to study the continuous variation from the 1-3 connectivity to the 2-2 connectivity, when the rods of the 1-3 configuration start to be in contact along only one given direction. As a result, a rule of mixture with a weighing coefficient *x*, can be defined between the θ parameter of the two connectivity patterns considered herein. It could be defined as: $\theta = x.\theta_{1\text{-}3} + (1-x).\theta_{2\text{-}2}$. This parameter is to be further established for various connectivity patterns, taking into account their specific boundary conditions. Therefore, expressions of θ are given as:

– For the 1-3 PCs

$$\theta = \bar{\nu}/[\nu(c_{11} + c_{12}) + \bar{\nu}(c_{11}^E + c_{12}^E)] = \theta_{1-3} \tag{37}$$

– For the 2-2 PCs

$$\theta = \bar{\nu}/[2\bar{\nu} c_{11}^E + \nu c_{11}] = \theta_{2-2} \tag{38}$$

For transducer applications, exact expressions for several key parameters are usually introduced, i.e. the for the acoustical impedance $\bar{Z}_L$, the longitudinal velocity $\bar{c}_L$ and the electromechanical coupling factor $\bar{k}_t$, are expressed as:

$$\begin{cases} \bar{Z}_L = (\bar{c}_{33}^D \bar{\rho})^{\frac{1}{2}} \\ \bar{c}_L = (\bar{c}_{33}^D / \bar{\rho})^{\frac{1}{2}} \\ \bar{k}_t = \bar{h}_{33} / (\bar{c}_{33}^D \bar{\beta}_{33}^S)^{\frac{1}{2}} = \bar{e}_{33} / (\bar{c}_{33}^D \bar{\epsilon}_{33}^S)^{\frac{1}{2}} \end{cases} \tag{39}$$

with

$$\begin{cases} \bar{\rho} = \nu \rho^c + (1-\nu)\rho^p \\ \bar{c}_{33}^D = \bar{c}_{33}^E + (\bar{e}_{33})^2 / \bar{\epsilon}_{33}^S \end{cases} \tag{40}$$

4 Results and discussion

The PZT-7A/Araldite D PC is used herein for numerical calculations. Table 1 summarizes its electromechanical characteristics [40].

Table 1 – Electromechanical characteristics of the PZT-7A/Araldite D PCs.

Materials	PZT-7A	Araldite D
c_{11}^E(GPa)	148.0	8.0
c_{12}^E(GPa)	76.2	4.4
c_{13}^E(GPa)	74.2	4.4
c_{33}^E(GPa)	131.0	8.0
c_{13}^D(GPa)	073.0	-
c_{33}^D(GPa)	175.0	-
$\epsilon_{33}^S/\epsilon_0$	235	4.0
$\epsilon_{33}^T/\epsilon_0$	425	4.0
e_{33}(C/m^2)	9.50	0
e_{31}(C/m^2)	–2.10	0
ρ(kg/m^3)	7600	1150
$\epsilon_0 = 8.854.10^{-12}$C^2/(Nm^2)		

In the previous section, we homogenized the 1-3 and 2-2 PZT-7A/Araldite D PCs properties. The homogenized characteristics of these PCs are plotted as a function of volume fraction of piezoelectric ceramics PZT-7A, for the 1-3 and 2-2 connectivities. The PZT-7A/Araldite D is chosen for comparison purposes with Chan's experimental data. The Voigt, and Reuss, models' results that give the upper and lower limits are used for comparison and validation. Figure 3a and Figure 3b show variations of the elastic constant $c_{33}^{E,eff}$ and the piezoelectric constant e_{33}^{eff}. The elastic constant ranges from 0 to 13 GPa. For the elastic constant, the upper limit is actually that of the Voigt model, and the lower limit is occupied by Reuss model. While for the piezoelectric constant, these two models are below 1-3 and 2-2 GHM. This result is in accordance with predictions found in the literature [17,41]. The two intermediate curves (i.e., between the Voigt and Reuss models) of fig3a, represent the proposed generalized homogenization plot for both patterns 1-3 and 2-2. Compared to various existing methods, the method proposed here can be used for different connectivities. For PZT-7A volume fractions lower than 10%, both curves coincide and evolve linearly.

For PZT-7A volume fractions ranging between 10% and 90% both curves also evolve linearly, but the results of the 2-2 Pcs are above that of 1-3. However, a sharp increase is observed in both curves. For the piezoelectric coefficients (fig3b), we observe that the Voigt model is inconsistent with either rule applied in the case of the elastic coefficients to obtain the upper limits, in the case of the 2-2 connectivity, but both models rather yield the lower limit of the piezoelectric coefficient. For the volume fractions lower than 10%, the curves obtained applying the generalized approach and the Reuss model are superimposed and evolve linearly. For volume fractions between 10 and 90% these curves also evolve linearly, and the results of the 1-3 PCs is above that of 2-2. With regard to the dielectric coefficients (fig3c), the curves are practically linear and coincide through the entire volume fraction range, while the Voigt model represents its lower limit. The PC electromechanical coupling coefficient, (fig3d) associated to the output of the transducer, should be carefully examined.

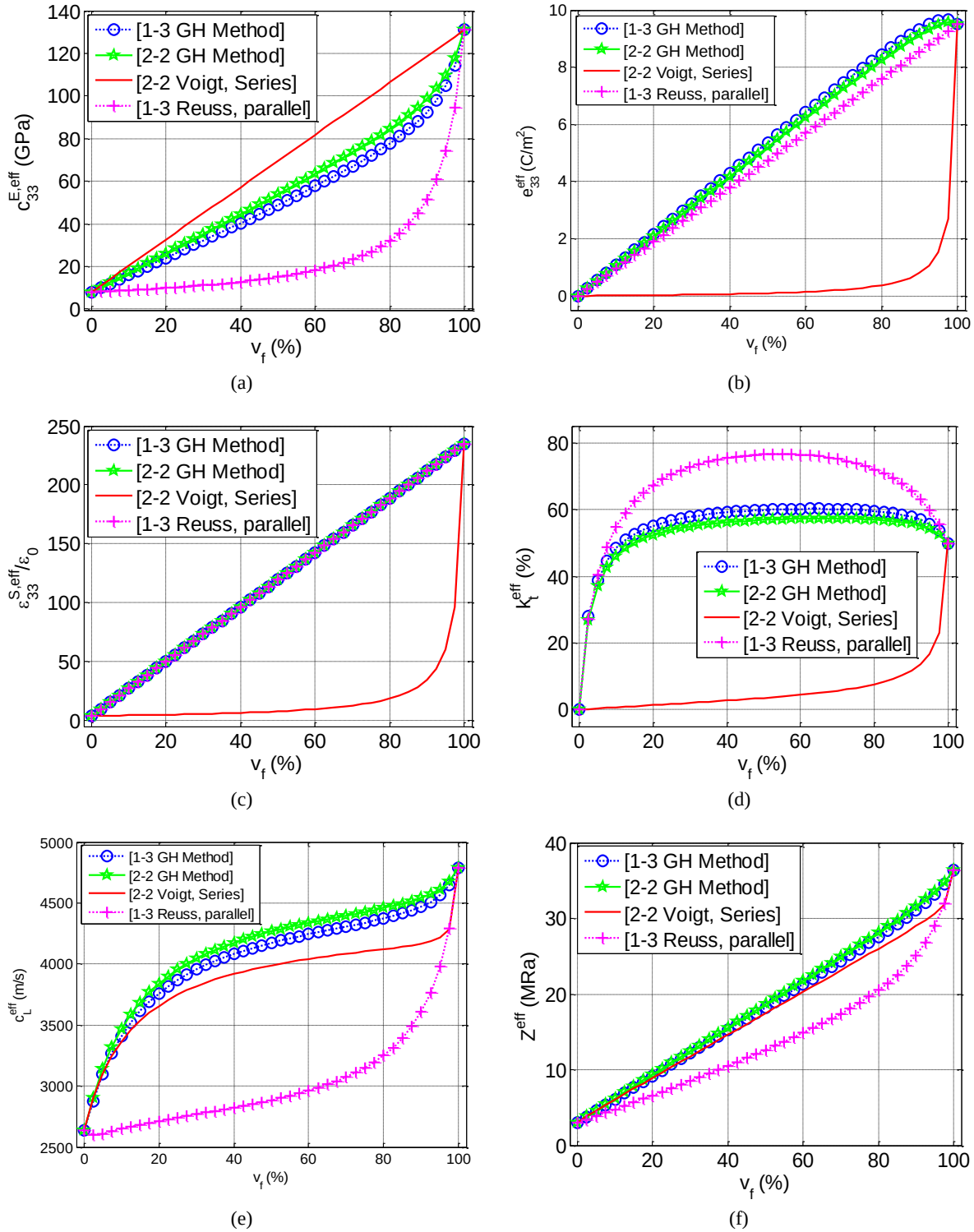

Figure 3 – Homogenized 1-3 and 2-2 Pcs with generalized model, made of PZT-7A/Araldite D as a function of volume fraction V_f of PZT-7A ceramics: (a) elastic constant $\bar{c}_{33}^{E}$, (b) piezoelectric constant $\bar{e}_{33}$, (c) relative dielectric constant $\bar{\epsilon}_{33}^{S}/\epsilon_0$, (d) electromechanical coupling constant $\bar{k}_t$, (e) longitudinal wave velocity $\bar{c}_L$ and (f) longitudinal acoustic impedance $\bar{Z}_L$.

For the 2-2 connectivity, applying the GHM, yields an electromechanical coupling greater than 50%. Whereas for the 1-3 connectivity, applying the GHM yields a value of 60%. As generally reported, the values of the electromechanical coupling of the 1-3 connectivity are above those of the 2-2 connectivity for volume fractions included between 5% and 90 %. This justifies the wide use of 1-3 PCs in manufacturing transducers. It should also be observed that the Reuss and Voigt models respectively represent the upper and lower limits. The acoustic impedances (fig3f) for the 2-2 connectivity obtained with the Voigt model represent the lower limit.

Likewise, the impedances obtained with the Reuss model for the 1-3 connectivity represents the lower limit. The acoustical impedance of 1-3 PC is lower than 2-2 PC due to its low elastic characteristics (1-3 PC is more elastic than 2-2 PC). As regards to the longitudinal velocity (fig3e) of 2-2 connectivity, we observe that the lower limit is the one of Voigt model derived velocity. Likewise, for 1-3 connectivity, the lower limit is the one of Reuss model derived velocity. These variations of the longitudinal acoustic wave velocity should not be neglected because it is important for the determination of the resonance frequency of the piezoelectric transducer made up of PCs of this work. The curves also suggest that the homogenized characteristics of the PCs depend on the models used as well as on the connectivity pattern of the PCs.

5. Comparison of the models

The GHM has been applied to the 1-3 and 2-2 PCs. Comparison is now made with the specific Smith's model for the 1-3 connectivity and Cha's model for the 2-2 connectivity. We compare results of various actual parameters of the PCs obtained using the GHM with the analytical models from Smith and Cha and with the experimental measurement extracted from the published work of Chan and Unsworth [40]. For the elastic coefficients with constant electric field (fig4a and fig4b) and piezoelectric coefficients (fig5a and fig5b), we notice that for 1-3 connectivity the generalized model is above that of the Smith model and that of the Cha model for the 2-2 connectivity. For the dielectric coefficients (fig6a and fig6b), we notice here that all the curves resulting from 1-3 and 2-2 connectivities are identical and evolve linearly. This explains why both connectivity patterns and even different methods used do not affect the dielectric coefficients. As illustrated by the thickness electromechanical coupling coefficient (fig.7a and fig7b), the GHM result is above that of the two specific Smith and Cha models.

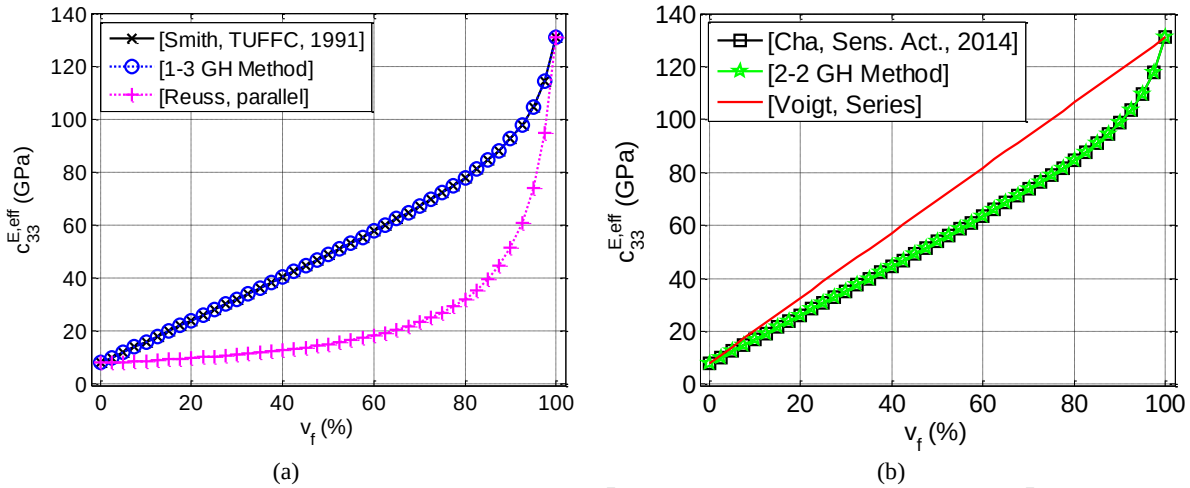

(a) (b)

Figure 4 – The GHM and analytical Smith and Cha models (a) $\bar{c}_{33}^{E}$ elastic constant of 1-3 connectivity, (b) $\bar{c}_{33}^{E}$ elastic constant of 2-2 connectivity.

For the 1-3 connectivity, the GHM result is above that of Smith and Cha models. As a result, in the case of 1-3 connectivities, the effective thickness coupling coefficient $\bar{k}_t$ (<50% for most of the ceramics) tends towards the k_{33} electromechanical coupling factor (>70% for optimized volume fractions). Eventually, unknown electroacoustic parameters of the transducer are: the longitudinal acoustic wave velocity (fig8a and fig8b) and the acoustical impedance (fig9a and fig9b). As illustrated, for 1-3 connectivity the generalized model is above that of Smith and Cha models of 2-2 connectivity.

For the elastic coefficients (fig4a and fig4b), for volume fractions lower than 15%, the model proposed here is linear and coincides with the Smith and Cha models.

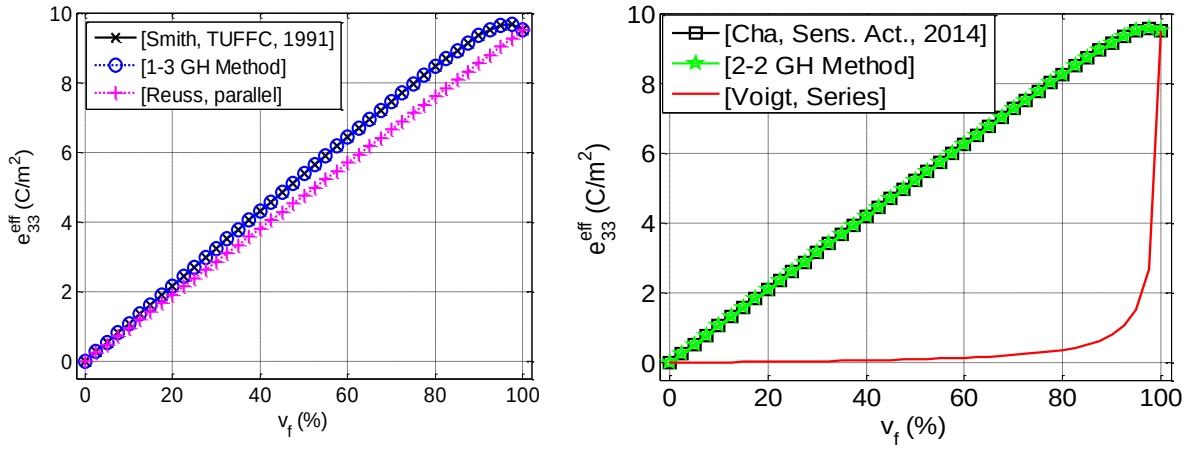

(a) (b)

Figure 5 – The GHM versus analytical Smith and Cha models (a) $\bar{e}_{33}$ piezoelectric constant of 1-3 connectivity, (b) $\bar{e}_{33}$ piezoelectric constant of 2-2 connectivity.

For volume fractions included between 15% and 80%, this model is linear and coincides with the Smith model whereas Cha model is above.

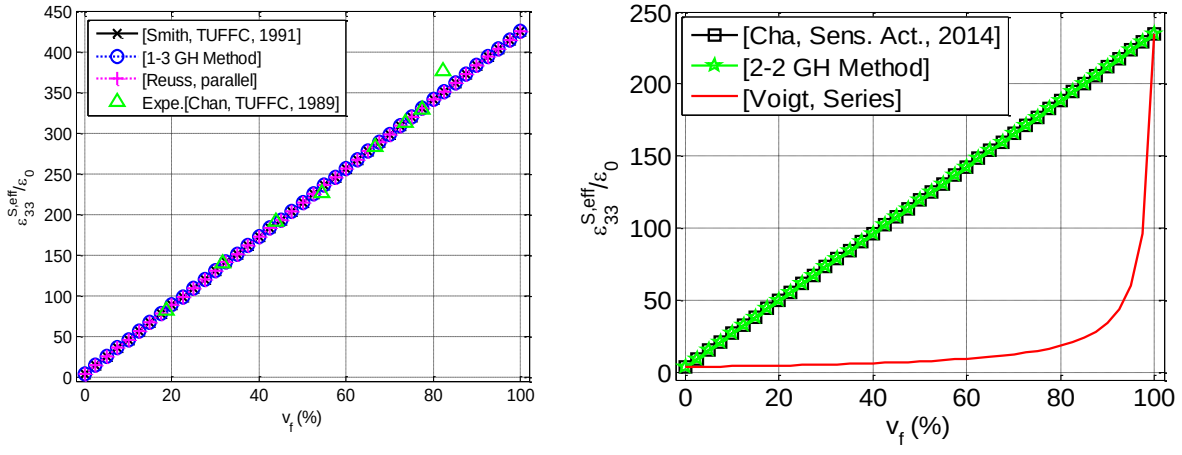

(a) (b)

Figure 6 – The GHM versus analytical Smith and Cha models (a) dielectric constant of 1-3 connectivity $\bar{\epsilon}_{33}^{S}/\epsilon_0$, (b) dielectric constant of 2-2 connectivity $\bar{\epsilon}_{33}^{S}/\epsilon_0$. The measured values are from Chan and Unsworth (1989).

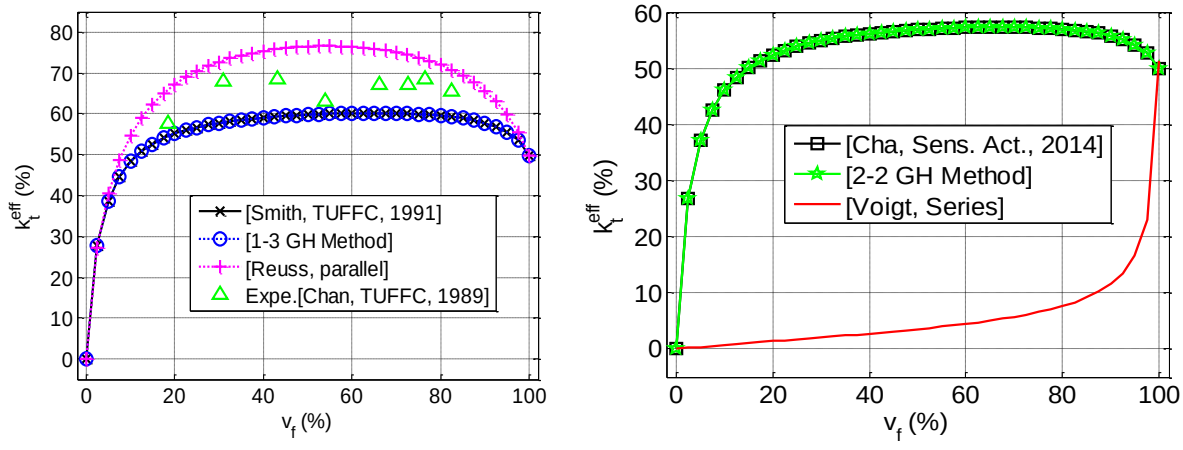

(a) (b)

Figure 7 – The GHM versus analytical Smith and Cha models (a) $\bar{k}_t$ electromechanical coupling coefficient of 1-3 connectivity, (b) $\bar{k}_t$ electromechanical coupling coefficient of 2-2 connectivity. The measured values are from Chan and Unsworth (1989).

This can be explained by the effect of the piezoelectric reinforcements on the stiffness of the material. For the piezoelectric coefficients (fig5a and fig5b), with volume fractions lower than 40%, this model is linear and coincides with the Smith and Cha models; between 40% and 90% the generalized model is always identical to that of Smith and higher than the Cha model. Dielectric coefficients curves (fig6a and fig6b), are linear and coincide for all the volume fractions. This can also be explained by the fact that dielectric coefficients are independent of connectivity pattern.

The thickness electromechanical coupling coefficient (figs7a-b), being related to the output of the transducer, it is observed that for small volume fraction values, this coefficient grows suddenly and coincide. For volume fractions included between 10% and 90%, this model is almost constant and coincide with the Smith model and both are above the Cha model. Eventually, for the longitudinal acoustic wave velocity (fig8a-b), and for volume fractions higher than 10%, this model shows an increase and coincide with the Smith model and both are below the Cha model, as also observed in the acoustical impedance plots (fig9a and fig9b). For the 1-3 connectivity and some parameters such as effective dielectric constant, longitudinal acoustical impedance and longitudinal wave velocity, we see that the generalized model result is in good agreement with experimental data extracted from Chan and Unsworth (1989), as well as other analytical results of Smith and Cha. For the electromechanical coupling factor, we notice that the measured values follow the pace of analytical curves, but these values are between the upper limit by Reuss parallel model and the GHM.

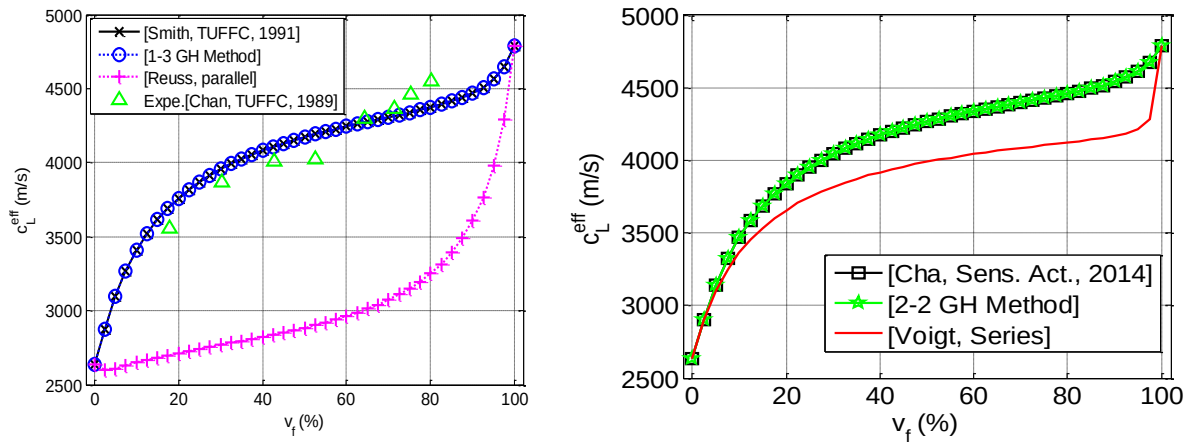

(a) (b)

Figure 8 – The GHM versus analytical Smith and Cha models (a) longitudinal wave velocity of 1-3 connectivity $\bar{c}_L$ and (b) longitudinal wave velocity of 2-2 connectivity $\bar{c}_L$.The measured values are from Chan and Unsworth (1989).

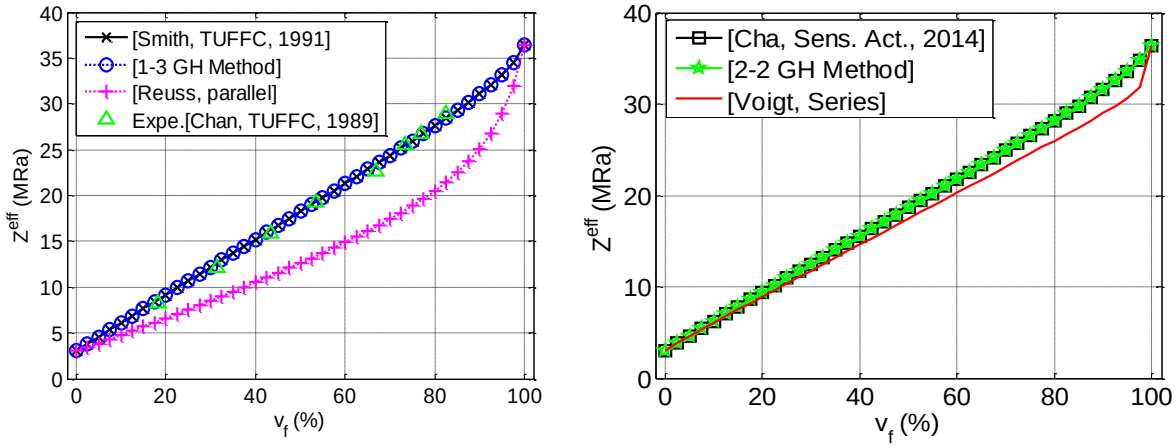

(a) (b)

Figure 9 – The GHM versus analytical Smith and Cha models (a) longitudinal acoustical impedance of 1-3 connectivity $\bar{Z}_L$ and (b) longitudinal acoustical impedance of 2-2 connectivity $\bar{Z}_L$.The measured values are from Chan and Unsworth (1989).

6. Transducer for medical imaging

Based on the GHM results of piezocomposite materials, the electroacoustic responses of transducers having some of these properties are simulated using the KLM model ([3], eq. (25)). The acoustic load is influencing the piezoelectric resonance, as well as the electrical environment. A three-port model is resulting from this approach, where two are acoustical ports (rear and front surrounding media) and one is an electrical port (electrical environment). In order to fix the parameter study, two of the three ports have been specified for an application in medical imaging. In this view, the design requirements are a front medium which is water with an acoustical impedance Z_f = 1.5 MRa, and an electrical environment fixed at $Z_g = Z_r$ = 50 Ω. The first thickness mode of the piezoelectric layer was chosen at f_0 = 40 MHz, with an active surface S = 50 mm^2. A specific trade-off between damping and sensitivity is obtained with the acoustical impedance of the backing Z_b relatively to that of the piezoelectric layer Z_p. Its effect is illustrated with a PZT-7A piezoelectric material, with $z_b = Z_b / Z_p$ varying from 0 to 1.5. As it can be observed, the bandwidth U_{rg} is broadened of the spectrum (fig10a) when the pulse-echo response is damped and shortened (fig10b).

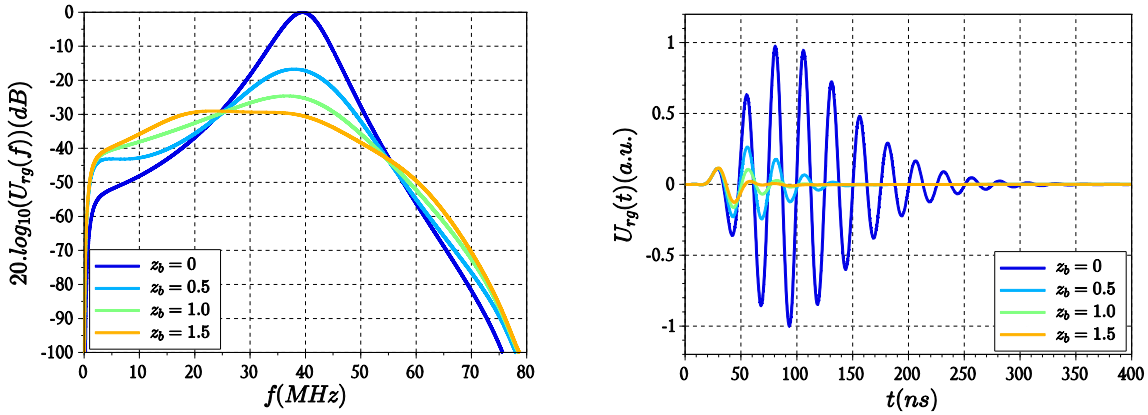

(a) (b)

Figure 10 – Pulse-echo (a) spectrum and (b) response resulting from a normalized backing impedance $z_b = Z_b / Z_p$ varying from 0 to 1.5, based on a PZT-7A piezoelectric material, with a thickness mode at f_0 = 40 MHz and an active surface S = 50 mm^2 radiating in water Z_f = 1.5 MRa, with an electrical environment fixed at $Z_g = Z_r$ = 50 Ω.

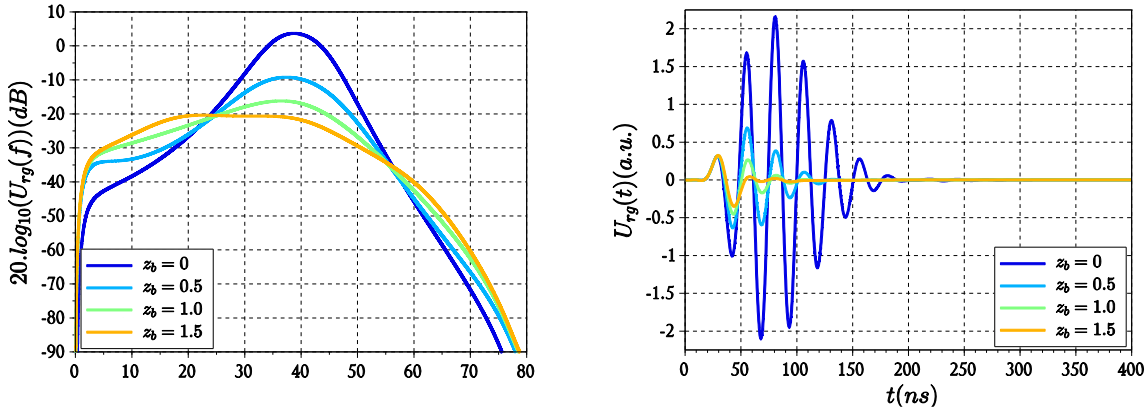

(a) (b)

Figure 11 – Pulse-echo (a) spectrum and (b) response resulting from a normalized backing impedance $z_b = Z_b / Z_p$ varying from 0 to 1.5, based on a GHM 2-2 piezocomposite material, with a thickness mode at f_0 = 40 MHz and an active surface S = 50 mm^2 radiating in water Z_f = 1.5 MRa, with an electrical environment fixed at $Z_g = Z_r$ = 50 Ω.

On the basis of the results from the GHM 2-2 configuration (fig4b to fig9b), a performance trade-off was chosen a v_f = 60%, resulting in an improved thickness coupling coefficient k_t = 57% and a lowered acoustical impedance $Z_{p,2\text{-}2}$ = 21.8 MRa. A similar approach as that on a pure PZT-7A shows a significant improvement of the transducer performance, which is illustrated both on the spectrum (fig11a) and the pulse-echo response (fig11b).

Tanks to the reduced acoustic mismatch between the piezocomposite and the front medium ($Z_f / Z_{p,2\text{-}2} = 0.069$ versus $Z_f / Z_{p,\text{PZT-7A}} = 0.041$), the sensitivity was increased by more than a factor 2 relatively to the same configuration with a PZT-7A piezoelectric element (fig11b) whatever the backing impedance. A specific trade-off between damping and sensitivity is to be fixed with a chosen normalized backing impedance. This choice can be assisted with the use of a performance index which has to be simple, stable and smooth, to be used as a fitting parameter in an optimization procedure [3]. Recently, the *BWA* product described in [18], was shown to fill those requirements. This *BWA* estimator results in the product of the relative bandwidth $BW_{6,r}$ by the relative amplitude amp_r, both extracted from the pulse-echo spectrum $U_{rg}(f)$:

$$BWA = BW_{6,r}.amp_r, \tag{41}$$

This comparison would also to be carried out with the GHM 1-3 piezocomposite optimum composition, which is also found at $v_f = 60\%$. Nevertheless, this is not mandatory nor relevant, since the effective properties for both connectivities are very close. As a perspective, a new composition is to be determined is view to highlight the interest of combining the 1-3 and 2-2 compositions. A mixing law between the GHM results is to be discussed for the two studied 2-2 and 1-3 configurations, with a θ parameter which can be set with intermediate values between $\theta_{1\text{-}3}$ (eq. (37)) and $\theta_{2\text{-}2}$ (eq. (38)) when the PC connectivity evolves between 1-3 and 2-2.

7. Conclusion

In this paper, a thorough review of existing homogenizations methods usually applied to PCs was carried out. It was observed that these models are essentially connectivity-oriented in computing effective characteristics. Therefore, we have developed a generalized homogenization method that accounts for Smith (1991) and Cha (2014) approaches to evaluate the equivalent characteristics of the piezocomposite. The proposed model can be applied to all connectivity patterns. However, this model has been only applied to 2-2 and 1-3 PCs herein. The GHM was used to compute the electromechanical coefficients of both the 1-3 and 2-2 connectivities when a parameter θ is changed to account for the pattern considered. Results obtained for some parameters show that the proposed GHM is consistent with the analytical existing models used for the 1-3 and 2-2 connectivities and is in line with measured values from Chan and Unsworth (1989). Based on the GHM 2-2 configuration results of piezocomposite materials, the electroacoustic responses of transducers having some of these properties are simulated using the KLM model. A performance trade-off was chosen, resulting in an improved thickness coupling coefficient and a lowered acoustical impedance, and a similar approach as that on a pure PZT-7A. Also, a specific trade-off between damping and sensitivity is obtained with the acoustical impedance of the backing relatively to that of the piezoelectric layer. Further work aiming to extend the applicability of the proposed model to other PCs connectivities patterns is anticipated. Accounting for the Smith homogenization approach θ expressions will be proposed for the remaining connectivities.

Funding sources
This research did not receive any specific grant from funding agencies in the public, commercial, or not-for-profit sectors.

Data Availability
Data will be made available upon request.

Conflict of interest
There are no conflicts of interest to declare.

References

[1] M.P. Thi, A.-C. Hladky-Hennion, H. Le Khanh, L.-P. Tran-Huu-Hue, M. Lethiecq, F. Levassort, Large area 0-3 and 1-3 piezoelectric composites based on single crystal PMN-PT for transducer applications, Physics Procedia. 3 (2010) 897–904.

[2] P. Marechal, F. Levassort, L.P. Tran-Huu-Hue, M. Lethiecq, Electro-acoustic response at the focal point of a focused transducer as a function of the acoustical properties of the lens, Proceeding of the 5th World Congress on Ultrasonics, 2003: pp. 535–538.

[3] P. Maréchal, F. Levassort, L.-P. Tran-Huu-Hue, M. Lethiecq, Lens-focused transducer modeling using an extended KLM model, Ultrasonics. 46 (2007) 155–167.
[4] D. Zhou, K.H. Lam, Y. Chen, Q. Zhang, Y.C. Chiu, H. Luo, J. Dai, H.L.W. Chan, Lead-free piezoelectric single crystal based 1--3 composites for ultrasonic transducer applications, Sensors and Actuators A: Physical. 182 (2012) 95–100.
[5] M. Racila, L. Boubakar, Composites piézoélectriques et homogénéisation asymptotique-Une approche numérique, Annals of the University of Craiova-Mathematics and Computer Science Series. 37 (2010) 99–124.
[6] C.N. Della, D. Shu, On the performance of 1-3 piezoelectric composites with a passive and active matrix, Sensors and Actuators A: Physical. 140 (2007) 200–206.
[7] C. Wang, Y. Liu, R. Zhang, W. Cao, Effect of kerf filler on the electromechanical coupling coefficient of 1-3 piezoelectric composites, Journal of Alloys and Compounds. 651 (2015) 643–647.
[8] W. Voigt, Lehrbuch der Kristallphysik,(1928), 962, BG Teuber, Leipzig. (1928) 962.
[9] A. Reuss, Berechnung der Fleissgrenze von Mischkristallen auf Grund der Plastizitats bedingung fur Einkrisalle, Zeitschrift Für Angewandte Mathematics Aus Mechanik. 9 (1929) 49–58.
[10] K.Y. Hashimoto, M. Yarnaguchi, Elastic, piezoelectric and dielectric properties of composite materials, IEEE 1986 Ultrasonics Symposium, 1986: pp. 697–702.
[11] F. Levassort, M. Lethiecq, D. Certon, F. Patat, A matrix method for modeling electroelastic moduli of 0-3 piezo-composites, IEEE Transactions on Ultrasonics, Ferroelectrics, and Frequency Control. 44 (1997) 445–452.
[12] F. Levassort, M. Lethiecq, R. Desmare, and L. P. Tran-Huu-Hue, Effective electroelastic moduli of 3-3(0-3) piezocomposites. IEEE Transactions on Ultrasonics, Ferroelectrics, and Frequency Control, vol. 46, no. 4, july 1999.
[13] W.A. Smith, B.A. Auld, Modeling 1–3 Composite Piezoelectrics: Thickness-Mode Oscillations, IEEE Transactions on Ultrasonics, Ferroelectrics, and Frequency Control. 38 (1991) 40–47. https://doi.org/10.1109/58.67833.
[14] J.H. Cha, J.H. Chang, Development of 15 MHz 2-2 piezo-composite ultrasound linear array transducers for ophthalmic imaging, Sensors and Actuators A: Physical. 217 (2014) 39–48.
[15] V.M. Levin, F.J. Sabina, J. Bravo-Castillero, R. Guinovart-Díaz, R. Rodríguez-Ramos, O.C. Valdiviezo-Mijangos, Analysis of effective properties of electroelastic composites using the self-consistent and asymptotic homogenization methods, International Journal of Engineering Science. 46 (2008) 818–834. https://doi.org/10.1016/j.ijengsci.2008.01.017.
[16] I. Elguesse, Etude et Application Des Composites A Base Des Matériaux Intelligents:(Cas Des Matériaux Piézoélectriques Et Des Alliages A Mémoire De Forme), (2015).
[17] F.L. Hanse Wampo, R.P. Lemanle Sanga, P. Maréchal, G.E. Ntamack, Piezocomposite transducer design and performance for high resolution ultrasound imaging transducers, IJCMS. 8 (2019) 1950013-48–48. https://doi.org/10.1142/S2047684119500131.
[18] P. Tize Mha, P. Maréchal, G.E. Ntamack, S. Charif d'Ouazzane, Homogenized electromechanical coefficients and effective parameters of 1–3 piezocomposites for ultrasound imaging transducers, Physics Letters A. 408 (2021) 127492. https://doi.org/10.1016/j.physleta.2021.127492.
[19] V.Y. Topolov, P. Bisegna, C.R. Bowen, Analysis of the piezoelectric performance of modern 0–3-type composites based on relaxor-ferroelectric single crystals, Ferroelectrics. 413 (2011) 176–191.
[20] V.Y. Topolov, C.R. Bowen, Electromechanical Properties in Composites Based on Ferroelectrics Vitaly Yuryevich Topolov Springer, (2009). https://www.springer.com/gp/book/9781848009998.
[21] V. Yu. Topolov, Figures of merit and problems of piezoelectric sensitivity of composites based on ferroelectric ceramics. WCU 2003, Paris, september 7-10, 2003.
[22] W. Qi, W. Cao, Finite element analysis and experimental studies on the thickness resonance of piezocomposite transducers, Ultrasonic Imaging. 18 (1996) 1–9.
[23] C. V Madhusudhana Rao, G. Prasad, Characterization of 1-3 piezoelectric polymer composites: a numerical and analytical evaluation procedure for thickness mode vibrations, Condensed Matter Physics. (2010).
[24] Y. Zhang, L. Wang, Q. Lei, Equivalent parameter model of 1-3 piezocomposite with a sandwich polymer, Results in Physics. 9 (2018) 1256–1261. https://doi.org/10.1016/j.rinp.2018.04.046.
[25] M. Sakthivel, A. Arockiarajan, Studies on effective fiber and matrix poling characteristics of 1-3 piezoelectric composites, The International Journal of Structural Changes in Solids. 3 (2011) 1–19.
[26] W. Li-kun, L. Li, Q. Lei, W. Weiwei, D. Tianxiao, Study of effective properties of modified 1-3 piezocomposites, Journal of Applied Physics. 104 (2008) 064120.
[27] L. Li, L.-K. Wang, L. Qin, Y. Lv, The theoretical model of 1-3-2 piezocomposites, IEEE Transactions on Ultrasonics, Ferroelectrics, and Frequency Control. 56 (2009) 1476–1482.

[28] G. Martinez-Ayuso, M.I. Friswell, S. Adhikari, H.H. Khodaparast, H. Berger, Homogenization of porous piezoelectric materials, International Journal of Solids and Structures. 113 (2017) 218–229.
[29] M.G.D. Geers, V.G. Kouznetsova, W.A.M. Brekelmans, Multi-scale computational homogenization: Trends and challenges, Journal of Computational and Applied Mathematics. 234 (2010) 2175–2182.
[30] H. Berger, S. Kari, U. Gabbert, R. Rodriguez-Ramos, R. Guinovart, J.A. Otero, J. Bravo-Castillero, An analytical and numerical approach for calculating effective material coefficients of piezoelectric fiber composites, International Journal of Solids and Structures. 42 (2005) 5692–5714.
[31] M. Avellaneda, P.J. Swart, Calculating the performance of 1–3 piezoelectric composites for hydrophone applications: an effective medium approach, The Journal of the Acoustical Society of America. 103 (1998) 1449–1467.
[32] M.L. Dunn, M. Taya, Micromechanics predictions of the effective electroelastic moduli of piezoelectric composites, International Journal of Solids and Structures. 30 (1993) 161–175.
[33] M.L. Dunn, M. Taya, Electromechanical properties of porous piezoelectric ceramics, Journal of the American Ceramic Society. 76 (1993) 1697–1706.
[34] J.D. Eshelby, The determination of the elastic field of an ellipsoidal inclusion, and related problems, Proc. R. Soc. Lond. A. 241 (1957) 376–396.
[35] R. Hill, Elastic properties of reinforced solids: some theoretical principles, Journal of the Mechanics and Physics of Solids. 11 (1963) 357–372.
[36] T. Mori, K. Tanaka, Average stress in matrix and average elastic energy of materials with misfitting inclusions, Acta Metallurgica. 21 (1973) 571–574.
[37] N. Pakam, A. Arockiarajan, Study on effective properties of 1-3-2 type magneto-electro-elastic composites, Sensors and Actuators A: Physical. 209 (2014) 87–99.
[38] R.E. Newnham, L.J. Bowen, K.A. Klicker, L.E. Cross, Composite piezoelectric transducers, Materials & Design. 2 (1980) 93–106.
[39] Y. Benveniste, G. Dvorak, Uniform fields and universal relations in piezoelectric composites, Journal of the Mechanics and Physics of Solids. 40 (1992) 1295–1312.
[40] H.L.W. Chan, J. Unsworth, Simple model for piezoelectric ceramic/polymer 1-3 composites used in ultrasonic transducer applications, IEEE Transactions on Ultrasonics, Ferroelectrics, and Frequency Control. 36 (1989) 434–441.
[41] J.Y. Li, M.L. Dunn, Variational bounds for the effective moduli of heterogeneous piezoelectric solids: Philosophical Magazine A: Vol 81, No 4, (2001). https://www.tandfonline.com/doi/abs/10.1080/01418610108214327.